scientific reports

Check for updates

OPEN

Airborne reflectors for satellite-based quantum entanglement and key distribution

Kavindu Sellahewa[1]✉, Nitish K. Panigrahy[2], Albert Williams[3], Don Towsley[3] & Deirdre Kilbane[1]

Satellite-based quantum communication faces challenges due to link intensity loss over long distances caused by various factors such as geometric loss and atmospheric attenuation. These effects can lead to lower entanglement distribution rates, secret key rates, and increased quantum bit error rates, especially in direct satellite-to-ground communication. This paper proposes a practical solution: the design of an airborne gold-coated parabolic reflector to be placed in the stratosphere directly above the ground station. This reflector effectively acts as a second virtual transmitter, a novel concept introduced in this work. The proposed method brings about a substantial increase in the distributed entanglement rate, boosting it by up to 25 times at zenith compared to direct satellite-to-ground communication. It also reduces the minimum elevation angle for secure communication, approximately from 28° to 18° for BB84 and from 36° to 22° for E91 when using the proposed reflector method compared to direct satellite-to-ground communication. Furthermore, the proposed reflector method extends the communication time window by 16.1% for the BB84 protocol and 25.9% for the E91 protocol. These enhancements underscore the potential of our approach to significantly extend the duration of secure communication and improve performance, particularly at lower elevation angles where direct satellite-to-ground communication is not feasible.

Keywords Quantum communications, Parabolic reflector, Satellite communications, Entanglement distribution, High-altitude reflectors, FSO communication

Quantum communication provides theoretically secure transmissions between end users based on laws of quantum physics[1]. Quantum Key Distribution (QKD) is the first and most practical branch of quantum communication[2], which shares a truly random key between end users, later used to encrypt messages securely. Extensive research has been carried out towards developing a global QKD network for this purpose, from a hybrid satellite and terrestrial QKD network in China[3] to a truly heterogeneous and scalable QKD network in Madrid MADQCI[4]. Recent advancements in quantum communication have also underscored the importance of entanglement distribution as a foundational element for protocols such as quantum teleportation[5], another main branch of quantum communication. In recent years, in addition to terrestrial networks, entanglement distribution using submarine optical fibres has also been demonstrated experimentally[6]. Instead of sharing keys for encryption, there is another branch in quantum communication, which directly shares the message by encoding into quantum bits known as Quantum Secure Direct Communication (QSDC)[7]. Conventional communication systems struggle with security risks, including key leakage to inside attackers. QSDC addresses these challenges by enabling the direct transmission of secret messages through a quantum channel. Since the information remains within the quantum domain, it is protected by the principles of quantum mechanics, ensuring unconditional security against unauthorised access or leakage[8]. Although quantum communication offers substantial security advantages, it necessitates the transmission of photons over long distances. However, the terrestrial quantum communication distance has currently been limited due to the exponential attenuation of light in fibre optic cables[9]. Currently, QSDC has been achieved over $300\ km$ experimentally[10]. Twin-field[11] is the most promising protocol for QKD over Long distances, reaching over 1000 km in laboratory experiments, which required ultra-low loss fibre, ultra-low noise superconducting nanowire single-photon detectors (SNSPDs), and time-multiplexed dual-band phase stabilisation[12].

[1]Walton Institute, South East Technological University, Carriganore, Waterford X91P20H, Ireland. [2]School of Computing, Binghamton University, PO Box 6000, Binghamton, NY 13902-6000, USA. [3]Manning College of Information & Computer Sciences, University of Massachusetts, Amherst, MA 01003, USA. ✉email: kavindu.sellahewa@waltoninstitute.ie

These limitations do not affect satellite-based quantum entanglement distribution, making it an attractive alternative for building secure global networks[13]. The Micius Low Earth Orbit (LEO) satellite was launched in 2016 to facilitate a series of quantum space experiments[14]. Pioneering missions included satellite-to-ground decoy state QKD with polarization encoding[14], the distribution of two entangled photons from a satellite to two ground stations separated by 1200 km[15]; quantum teleportation of single-photon qubits from a ground observatory to the Micius satellite over a distance of 1400 km[16]; and intercontinental quantum communications over a distance of 7600 km enabling secure videoconferencing between China and Austria[17]. However, satellite-based quantum communications face several significant challenges regarding the intensity of the communication link and the time required for distributing quantum keys, as outlined below[9].

- Limited line of sight time window for non-geostationary satellites. (This time is further reduced by the minimum elevation angle of 5° requirement to initiate the communication link and at least 10° for a stable connection[18].
- Intensity loss due to the beam divergence of the quantum link over large distances.
- Signal attenuation due to atmospheric turbulence, weather conditions, and cloud coverage.
- Other losses due to pointing errors and Doppler shift of wavelength

Even though some environmental factors mentioned above that reduce intensity, like atmospheric turbulence and cloud blockage, are out of human control, they have been addressed in various ways. For example, having multiple ground stations can help to deal with cloud blockages as it creates site diversity[19] where a ground station with a clear sky can communicate with a satellite while others cannot. On the other hand, numerous successful attempts have been initiated to deal with background noise and atmospheric turbulence conditions as well[19,20]. Recent reviews summarise the significant advances made in satellite QKD (SatQKD)[21,22]. These include theoretical modelling of losses due to atmospheric effects[23–25], simulation software for analyzing the performance of various QKD protocols using optimization routines and asymptotic expressions[26], and the design of advanced adaptive optics systems to minimize atmospheric losses[27]. Indeed, ground-based horizontal field trials have taken place which combine adaptive optics systems with spatial, spectral and temporal filtering to allow for daylight operation[28].

However, It is crucial to tackle other challenges, such as extending the communication time window while enhancing Entanglement Distribution Rate (EDR) along with Secret Key Rate (SKR) and reducing Quantum Bit Error Rate (QBER). SKR represents the amount of information (in bits) available for encryption after eliminating errors or leaked information to an eavesdropper during each communication opportunity. QBER is a key metric in quantum communication and is an estimate of the percentage of errors in the key receiving process. A lower QBER indicates a higher quality of the quantum channel, as fewer bits are lost to noise or tampering. QKD protocols such as BB84[29] and E91[30] also play a central role as they offer different SKR, QBER and security levels even under the same loss conditions. BB84 is a protocol that uses polarized photons to encode information in different bases, and the secure key generation relies on the laws of quantum mechanics, particularly the inability of an eavesdropper to measure quantum states without disturbing them. E91, on the other hand, is based on the distribution of entangled photon pairs and the violation of Bell's inequality, quantified by Bell's parameter. When Bell's parameter exceeds a certain threshold, it indicates the presence of quantum entanglement, enabling the establishment of secure key distribution.

This paper addresses two of the limitations mentioned above: low EDR along with SKR and short communication time with non-geostationary satellites. The proposed system is a gold-coated parabolic reflector carried by a high-altitude balloon floating in the stratosphere, positioned directly above the ground station. This design, acting as a receiver from the satellite, is a highly reliable solution that establishes stable communications with the satellite, even when the ground station cannot do so directly (i.e., at lower elevation angles). It extends the total duration of the communication window, providing a reliable and consistent connection. Consistently placing the reflector at a 90° elevation angle with the ground station helps achieve the lowest possible link loss while transmitting through the dense layer of the atmosphere, increasing EDR and SKR. The parabolic design of the reflector also increases signal directivity, allowing the ground station to receive a relatively low-diverging beam compared to direct communication, thereby allowing lower-aperture telescopes as receivers, which are available commercially. Although the feasibility of using High Altitude Platforms (HAPs) for quantum key distribution has been studied previously[1,31], this is the first time that parabolic reflectors on HAPs have been proposed as virtual transmitters in satellite-based quantum communications to the best of our knowledge.

We evaluate our method by measuring the average EDR without any QKD protocol involved along with SKR, QBER, and communication time with both the E91 and BB84 protocols. Additionally, we analyze the Bell parameter value to determine the level of entanglement violation after implementing the E91 protocol. All of these evaluation methods are carried out under three different scenarios as follows. In the first scenario, Case I, the HAP is a quantum link reflector from the satellite to the ground station. In the second scenario, Case II, the HAP is a trusted end node between the satellite and the ground station. The HAP securely communicates with the ground station to distribute the quantum key via classical channels after receiving it from the satellite, demonstrating a hybrid situation. The third scenario, Case III, is the standard SatQKD approach with direct quantum communication from the satellite to the ground station. The design in Case I and II has the potential to significantly impact satellite communication and antenna design, inspiring further innovation in the field. In fact, dynamic switching between all 3 scenarios could be used to maximize the overall performance of quantum communication via satellite.

Results

SatQKD via parabolic refelctors

Parabolic antennas have a wide range of applications, including radio astronomy, satellite communications, and microwave communications[32] due to their high gain and directivity. According to geometrical optics, when a parallel ray series is incident upon a parabolic reflector, its overall radiation characteristics converge to the reflector's focal point[33]. Placing a feed horn at the focal point, known as the front feed, is one method of detecting the amplified and focused signal by the reflector (Fig. 1), which will be utilised in this paper.

The directivity of an antenna indicates the amount of signal power concentrated in a specific direction[34]. In the context of a parabolic reflector, this directivity represents how effectively the transmitting reflector (Fig. 1) focuses outgoing optical waves parallel to its central (principal) axis. A highly directive antenna sends more of its energy in a narrow angular region, minimising spread and maximising the photon transfer in that direction. This is crucial in quantum communications to minimise QBER, as a larger number of photons leads to a more robust reading of the encoded information, which reduces the likelihood of error introduced by noise, atmospheric interference, or detector inefficiencies (i.e., a better signal-to-noise ratio). Conversely, a lower photon count can increase the QBER, making the quantum communication link less secure and unreliable. The signal directivity (in dB) of a parabolic reflector is mathematically defined as follows:

$$D_0 = 10 \cdot \log((\pi d/\lambda)^2 \epsilon_{\mathrm{ap}}) \tag{1}$$

Here, d is the reflector's diameter and λ is the signal wavelength. The term ϵ_{ap} is the aperture efficiency, representing the fraction of the physical aperture area that effectively contributes to beam formation. According to equation (1), a larger diameter or a shorter operating wavelength (optical waves compared to radio waves) results in a narrower and more focused beam, thereby increasing the signal's directivity. Intuitively, this means that the antenna can concentrate more energy in the direction it is pointing, which is crucial for long-distance optical links, such as HAP-to-ground quantum communication. The term ϵ_{ap} can be further divided as,

$$\epsilon_{\mathrm{ap}} = \epsilon_{\mathrm{s}} \epsilon_{\mathrm{t}} \epsilon_{\mathrm{p}} \epsilon_{\mathrm{x}} \epsilon_{\mathrm{r}} \tag{2}$$

where $\epsilon_s, \epsilon_t, \epsilon_p, \epsilon_x, \epsilon_r$ are spillover, taper, phase, polarisation, and random error efficiencies, respectively. These parameters represent loss due to imperfections in the construction and unaccounted-for random environmental conditions. However, as a more general value, ϵ_{ap} is set to 0.65, which is typical for a well-constructed antenna[35].

As shown in Fig.1, we use two parabolic reflectors in our design to receive and redirect the quantum signal back to the ground station. Considering a transmitter reflector with a diameter of 0.3 m and a quantum signal wavelength of 1550 nm (values utilised in our proposed design), we calculate the transmitter's directivity (inversely proportional to the beam divergence) to be 114.09 dB. This results in a substantial increase in concentrated power delivered to the ground station than provided by direct satellite communication, which experiences considerable beam divergence. Geometric loss occurs due to natural beam widening, typically a significant loss. This loss L_{GEO} is (in dB)[1],

$$L_{GEO} = 20 \cdot \log_{10}((D_t + l_{path} \cdot w_o)/D_r), \tag{3}$$

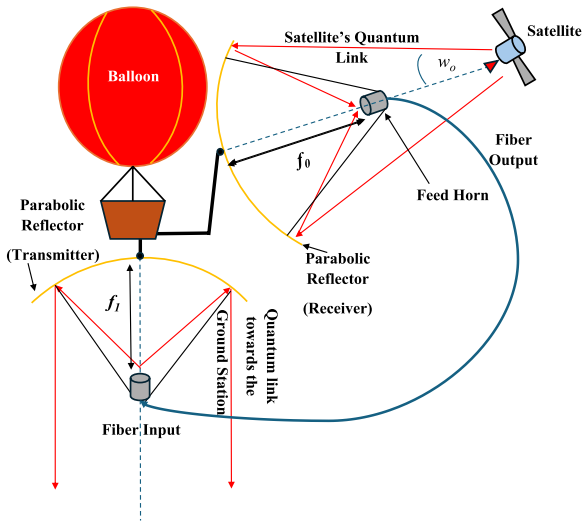

Fig. 1. High reflectivity, gold-coated parabola design acting as a receiver to the satellite and a transmitter to the ground station. f_0 and f_1 are the focal points of the receiving and transmitting parabolas, respectively. Due to practical reasons, such as beam divergence, the actual focal point can be slightly changed from the geometric focal point of the parabola. The figure is not in scale.

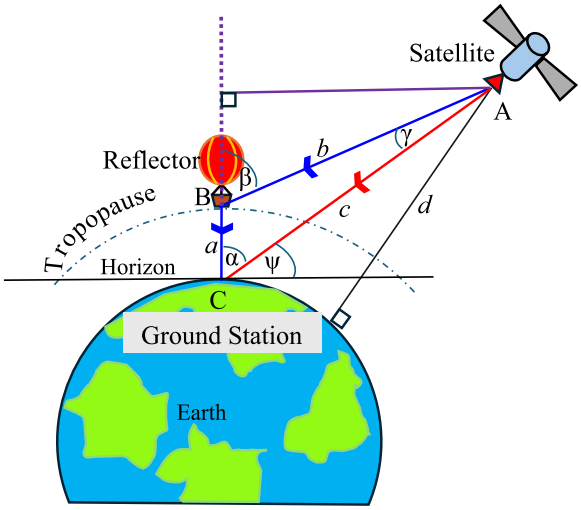

Fig. 2. A snapshot of the satellite's sighting to compare the three scenarios. Here, β is the zenith angle between the balloon and the satellite, α is the zenith angle between the ground station and the satellite, $a(= 20\ km)$ is the height of the balloon, *b* is the line of sight distance, from the balloon to the satellite, *c* is the line of sight distance from the ground station to the satellite, and *d* is the altitude of the satellite and ψ is the elevation angle of the satellite as seen by the ground station (with the horizon). l_{path} can be either *a*, *b* or *c* depending on the communication route. Refer to supplementary materials for calculations of *b* and β (figure is not in scale).

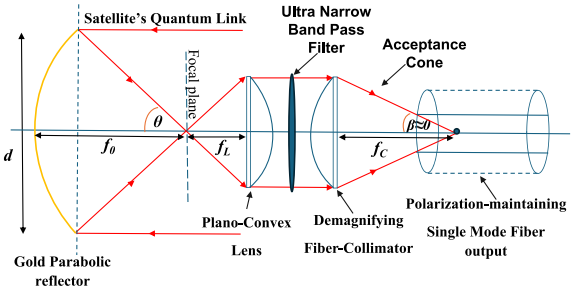

Fig. 3. The optical element structure inside the parabola's feed horn. Here, the feed horn is placed so that the focal length of the first plano-convex lens coincides with the focal plane of the reflector. f_o is the focus point of the parabolic reflector, *d* is the diameter of the reflector, f_L is the focal length of the plano-convex lens, and f_C is the focal length of the collimator. The bandpass filter is only used in the receiver system to filter the noise. The central wavelength of the filter is $1550 \pm 10nm$. (The figure is not in scale).

where l_{path} is the line of sight distance in meters (m), D_t and D_r are the diameters of the transmitter and the receiver, respectively (also in m), and w_o is the half beam divergence. Here w_o is,

$$w_o = 1.22\lambda/D_t. \tag{4}$$

According to geometry, the radius of the receiving light cone at the ground station is the product of $\tan\omega_o$ and the line of sight distance, l_{path}. Since ω_o is very small, $\tan\omega_o \approx \omega_o$, which gives the beam radius as $\omega_o \cdot l_{path}$. For example, with the same ω_o for the satellite and reflector transmitters (as λ and D_t do not change for both transmitters (equation (4)), at $\psi = 90°$, the beam width ratio between direct satellite link and the link redirected by the reflector is $l_{path}(AC) : l_{path}(BC) = 430 : 20$ (Fig. 2). Which means the beam width of the direct satellite link at the ground station is 21.5 times larger than the link redirected by the reflector.

Combined with this higher directivity of the antenna and the almost pure signal wavelength provided by the onboard optical system, as shown in Fig. 3, the transmitting parabola on the balloon can be considered a virtual laser source. This allows us to treat it as a new, separate transmitter when calculating the channel loss between the balloon and the ground station.

Effect of the gold coating

Gold is one of the best available reflectors for infrared (IR) applications, with a reflectivity of about 0.98 at 1550 nm[36], the wavelength to be used in this paper. Consequently, there is growing interest in gold-coated parabolic reflectors in both quantum[37] and non-quantum[36] research fields. Symmetric parabolic reflectors are designed

to minimize cross-polarization effects when illuminated with balanced polarized light[38], as this alignment ensures minimal deviation in the reflected polarization state. Furthermore, using gold coating, known for its high reflectivity at quantum communication wavelengths (e.g., 1550 nm), helps preserve the fidelity of quantum states by reducing scattering and absorption losses. These factors collectively contribute to a very low probability of damaging the encoded quantum information in such links. The above statement is further supported by experimental evidence demonstrating very low quantum defects caused by highly reflective materials[39,40]. However, it is essential to note that the reflection properties of materials change with temperature. A study has shown that the reflectance of gold decreases slightly at higher temperatures for wavelengths greater than or equal to 500 nm[41]. This is not a limitation in our application as the reflector is in the stratosphere, where low-temperature conditions occur.

Channel loss

We assume a laser onboard a LEO satellite as the transmission source in our simulations due to practical reasons. These include low launching costs, extensive geographic coverage, and the availability of actual satellites dedicated to quantum communication already in orbit[42]. To facilitate comparison, we calculate the total channel loss experienced during satellite-to-ground station transmission under three scenarios described in Sect. "Introduction". The total channel loss L_{TOT} (dB) is presented in detail in Sect. "Methods" and, for a certain l_{path} (Fig. 2), can be expressed as,

$$L_{TOT} = L_{GEO} + L_{ATM} + L_{PNT} + L_{SCI} \tag{5}$$

where L_{ATM} is the atmospheric loss, L_{PNT} is the pointing loss, and L_{SCI} is the scintillation loss as will be described in Sect. "Methods".

Use cases

In this paper, we consider two use cases for the parabolic reflector and compare them against the baseline, which is direct satellite-to-ground communication as described in the Methods. The first use case (balloon as a quantum link reflector) improves the performance of various quantum applications such as quantum sensing, distributed quantum computing, and QKD. The second use case (ballon as quantum receiver) is a hybrid method suitable for QKD but not for entanglement distribution. QKD is still possible with post-quantum cryptography. Both methods perform better than direct satellite communication with the ground station.

All three scenarios apply identical environmental and systematic conditions to ensure a comprehensive and equitable comparison. All parameters utilised in this comparative analysis are documented in Table 1. As the first step, we calculate the total loss under each scenario. Then SKR and QBER for BB84 and E91 (along with the Bell parameter for E91), EDR, and time window calculations are discussed in Sect. "Performance analysis". Losses and rates are calculated for each of the three scenarios for a range of elevation angles, and findings are discussed.

Case I: Rerouting through the reflector

In this case, the reflector is positioned in the stratosphere and is used to calculate the performance metrics where quantum information travels on the path AB+BC (Fig. 2). The total loss on this travel path L_{ABC} is

$$L_{ABC} = L_{T-AB} + L_{ref} + L_{T-BC} \tag{6}$$

where L_{T-AB} and L_{T-BC} are the total channel losses for travel paths AB and BC (Fig. 2), respectively calculated using equation (5) for each case. We assume the ground station sees the balloon as a new transmission source as explained in Sect. "SatQKD via parabolic refelctors", which is always at 90° elevation to the ground station when considering the travel path *BC*. L_{ref} (in dB) is the loss introduced by the reflector due to its imperfections presented in Sect. "Methods" calculated as

$$L_{ref} = L_{coating} + L_{lenses} + L_{design} + L_{fibre} \tag{7}$$

Here, L_{fibre} (given in equation (20)) represents the loss due to the attenuation inside the fibre optic cable and coupling inefficiencies, $L_{coating}$ (given in equation (21)) is the loss due to imperfect reflection by the

Description	Value	Description	Value
Transmitter's aperture (satellite)	0.3 *m*	Transmitter's aperture (balloon)	0.3 *m*
Receiver's aperture (balloon)	2 *m*	Receiver's aperture (ground)	0.4064 *m* (16")
Signal wavelength (λ)	1550 *nm*	Altitude of the satellite (d)	430 *km* (LEO)
Pointing jitter (θ_j)	5 μrad	Wind speed (high turbulence)	20 *m/s*
RISP at ground (A_0)	$1 \times 10^{-15} m^{-2/3}$	Height of ground station (H_{GS})	0.01 *km*
Reflectance of gold (r)	0.98	Optical efficiency of lenses (t)	0.9
Noise count probability (P_{nc})	1×10^{-5}	Detector efficiency (η_{det})	0.8
Photon generation rate (ν_s)	5.9 *MHz*	Number of detectors (BB84)	2

Table 1. Parameter description and respective values used in the simulation.

coating, L_{lenses} (given in equation (22)) is the loss due to imperfect transmission by the lens system (Fig. 3), L_{design} (given in equation (23)) is the loss due to misalignment as the beam diverges, design and environmental mismatches such as thermal fluctuations. We neglect fibre attenuation in our calculations as the fibre optic connectivity from the receiving reflector to the transmitting reflector is very small (about 10 m).

Case II: Hybrid communication (quantum + classical)
In Case-II, the balloon acts as a trusted end node to receive the key, which is transmitted classically to the ground station with one-time padding[43] (assuming no eavesdropping on the classical channel) where the quantum link travels on the path AB. In this case, we do not consider loss due to travel path BC, as it is classical communication, but only the loss on path AB (Fig. 2). Furthermore, the loss due to the reflector is half the amount in the previous case (the reflector method), as there is only one parabolic setup without the transmitter. Considering these factors, the loss in the hybrid scenario L_{AB} can be calculated as,

$$L_{AB} = L_{T-AB} + \frac{L_{ref}}{2} \tag{8}$$

Case III: Direct communication with the satellite
The baseline (Case-III) involves direct communication with the ground station, representing the conventional approach (the quantum link's path is AC or the red line in Fig. 2). Calculating the loss under direct communication is straightforward compared to the other two methods. Here, we can directly calculate the path loss from A to C, L_{AC} (Fig. 2), using equation (5) for different elevation angles shown in Sect. "Performance analysis".

Performance analysis

While this paper is mainly focused on entanglement distribution, we also consider SKR and QBER as performance metrics with BB84 protocol as well in addition to E91 protocol to demonstrate the usage in other QKD applications, too. Furthermore, we also perform Bell parameter analysis with the E91 protocol to demonstrate that entanglement violation is decreased with the introduction of the parabolic reflector.

Quantum signals undergo various losses during transmission from the satellite to the ground station. This paper focuses on geometric, atmospheric, pointing, and scintillation losses (together referred to as channel loss in this paper) and how they are calculated when finding the above-mentioned performance metrics, as described in Sect. "Methods".

Channel loss analysis
Since the above performance metrics depend on channel loss, we analyze the total channel loss along the propagation paths in all three scenarios (Case-I, II, and III) using the equations presented in Sect. "Methods". Channel loss as a function of the elevation angle of the satellite to the ground station, ψ (since $\beta \approx \psi$ as $a << d$), is presented in Fig. 4.

SKR and QBER analysis
Figure 5 depicts the SKR and QBER for the BB84 and E91 protocols. Both protocols demonstrate a noteworthy increase in SKR after introducing the parabolic reflector design compared to the baseline. With direct communication, the BB84 protocol exhibits a dead angle limit of $\approx 28^\circ$ for the simulation parameters given in Table 1. This increases to around $\approx 36^\circ$ for the E91 protocol. At the same time, the reflector method allows communication from $\approx 18^\circ$ for the BB84 protocol and $\approx 22^\circ$ for the E91 protocol. In contrast, the hybrid communication method allows communication from $\approx 14^\circ$ for the BB84 protocol and $\approx 18^\circ$ for the E91 protocol.

EDR analysis
Figure 6 represents the average entanglement distribution rate to the ground stations by considering both ground stations, Alice and Bob, using the expression for EDR given by equation (33). In this case, only the reflector

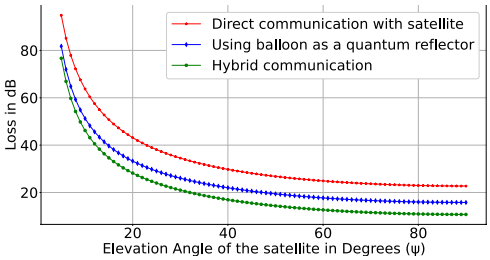

Fig. 4. The loss (in *dB*) for reflector, hybrid, and direct methods. The X-axis shows the elevation angle of the satellite as seen by the ground station (i.e., ψ in Fig. 2). Blue Curve: Reflector Method (Case I), Green Curve: Hybrid Communication (Case II), Red Curve: Direct Communication (Case III). (The results in this section are derived based on the assumption of a 2 *m* (aperture) parabolic receiver on the balloon. For a comparative analysis of these parameters across varied sizes of parabolic receivers, please refer to the supplementary materials.

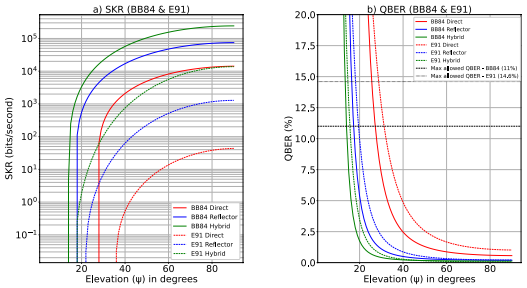

Fig. 5. SKR (**a**) and QBER (**b**) analysis for the BB84 (solid lines) and E91 (dashed lines) protocols as a function of elevation angle ψ. Blue lines represent the reflector method (Case I), green lines represent hybrid communication (Case II), and red lines represent direct communication (Case III). The maximum allowed QBER for BB84 is 11%[44] while it is 14.6 for the E91 protocol.

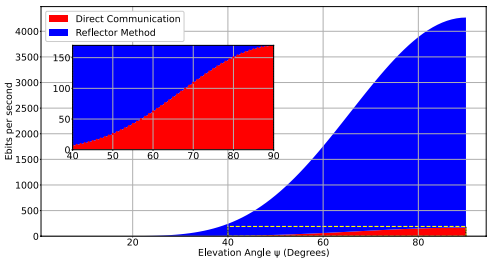

Fig. 6. This graph compares the EDR to the ground stations (measured in bits per second) of the direct method (red area) and the reflector method (blue area) as a function of elevation angle ψ (expressed in degrees). The accompanying subplot highlights the values of EDR associated with direct communication, which are contained within the boundaries of the yellow dashed-line box (for $40^\circ \leq \psi \leq 90^\circ$).

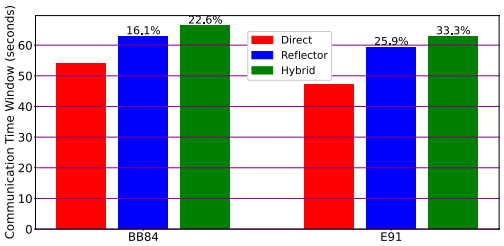

Fig. 7. Length of the communication time window (for $0^\circ \leq \psi \leq 90^\circ$) analysis for direct (red), reflector (blue), and hybrid (green) communications for both BB84 (left group) and E91 (right group) protocols. The increased percentage of the communication time window is marked on the top of the reflector (Case I) and hybrid bars (Case II) compared to the direct communication (Case III) for each protocol individually.

and direct methods (Cases I and III) are considered, as the hybrid communication method does not support entanglement distribution between a balloon and a ground station. The reflector method supports around 25 times more entangled bits to be distributed than direct communication at the maximum elevation angle (i.e., $\psi = 90^\circ$). The subplot highlights the entanglement generation rate for the direct communication scenario.

Communication time window comparison

A LEO satellite orbiting at an altitude ranging from 400 - 800 *km* typically has an angular velocity of 20 $mrad\ s^{-1}$ [45], relative to the receiver (balloon or ground station in our case) in its local coordinate system. Using equation (34) and the θ_{min} values extracted from Fig. 5, communication time windows can be calculated for each protocol, as shown in Fig. 7. It also shows the increased communication time as a percentage when using the reflector and hybrid methods compared to direct communication for both protocols. The reflector method provides 16.1% and 25.9% communication time increments for BB84 and E91, respectively, while the hybrid method provides 22.6% and 33.3% increments for BB84 and E91, respectively.

Bell parameter analysis

In the case of the E91 protocol, successful entanglement requires the Bell parameter to fall between 2 (classical limit) and $2\sqrt{2}$ (the ideal scenario). Any value below 2 suggests interference from an eavesdropper or excessive noise. According to equation (30), it is evident that QBER values exceeding 14.6% in the E91 protocol do not allow the generation of a secret key, as the Bell parameter falls below 2, the classical limit. This situation is demonstrated in Fig. 8, which illustrates the variations in the Bell parameter as a function of the satellite's elevation angle (ψ) for all three cases. Our approach provides a promising level of security even at lower elevation angles, at least from around 14.6° with the hybrid method and around 18° with the reflector method, where direct communication fails to do so, thereby increasing the communication time window.

Discussion

Our proposed airborne reflector scheme has several advantages beyond increasing communication times, entanglement distribution rates, and secret key rates. Our simulations utilised a two-meter, large-diameter parabolic receiver on the balloon, but a readily available 16-inch, small-aperture telescope at the ground station. This choice eliminates the need for custom-made or expensive high-aperture telescopes at ground stations in satellite-based quantum key distribution, making the method more practical and accessible. Supplementary materials present results for different diameters of the receiving parabola on the balloon.

For comparison purposes, we consider the total channel loss (returned by equation (5)) of the reflector method while having a 16-inch telescope at the ground station with the direct satellite-to-ground communication while having $1\ m$ receiver telescope (a common interest when considering real-world applications) at the ground station. We observe that having a $1\ m$ telescope provides slightly better performance (without involving reflector) for $\psi \geq 17^\circ$. Although this is the case, these results were obtained by assuming a parabola with $\epsilon_{ap} = 0.65$, which is a front feed design. There are more efficient designs, such as off-axis feed, which can provide an ϵ_{ap} value of up to 0.8[46]. Assuming $\epsilon_{ap} = 0.8$, the reflector method still provides a lower total channel loss (Refer to supplementary materials for loss analysis curves) while rerouting through it with a 16-inch telescope at the ground station compared to direct satellite-to-ground communication with a $1\ m$ telescope at the ground station. Future work should investigate a detailed analysis of an efficient parabolic reflector design and its performance under various environmental conditions.

However, our design exhibits some limitations and challenges. A major concern is the weight limitation a HAP can handle when designing the reflector setup, which affects the launch cost. Although the project Loon demonstrated the capability of carrying a payload of 28.5 *kg* into the stratosphere using a high-altitude balloon[47], our design can further reduce the manufacturing and launching costs by using lightweight materials to build reflectors instead of traditional metal dishes. Another concern is the stability of the balloon; however, this is less of a concern at a 20 *km* altitude as there are almost no rapid and strong wind currents. Furthermore, our study assumes that the reflector does not directly face the sun due to safety concerns regarding onboard equipment and to maintain a favourable signal-to-noise ratio, which may impose some communication time restrictions during daytime. Additionally, it is assumed that the reflector tracks the satellite actively, consistently maintaining direct alignment with it, backed by a mechatronic system.

Methods

Propagation losses

This section describes how each loss component (geometric, atmospheric, *etc.* as below) is calculated, which contributes to the total channel loss for travel paths ABC (Case-I), AB (Case-II), and AC (Case-III) (Fig. 2).

Atmospheric loss

Atmospheric loss occurs for two main reasons: the first is due to absorption by carbon dioxide molecules and water vapor[48]. The second is due to weather conditions such as snow, rain or fog. In the current model we assume clear conditions in our simulation, only taking the absorption loss into account. Then the atmospheric loss L_{ATM} (in *dB*) can be calculated as,

$$L_{ATM} = f_{loss} \times l_{path} \times 10^{-3} \tag{9}$$

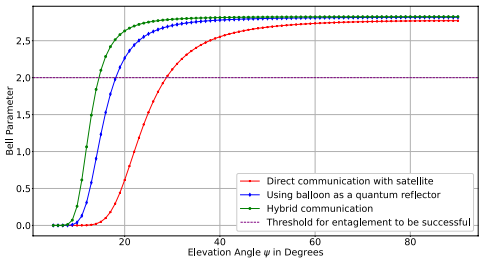

Fig. 8. Variation of the Bell parameter for the reflector, hybrid, and direct communication methods with the elevation angle of the satellite as seen by the ground station. The purple line represents the classical limit where the Bell parameter must lie above this limit for the entanglement to be successful.

where f_{loss} is the loss factor (in $dB\ km^{-1}$). However, the loss factor differs by the wavelength, and for 1550 nm, it is estimated to be $0.01\ dB\ km^{-1}$[1]. In this equation, l_{path} is multiplied by 1×10^{-3} to convert into *km*, as it was defined in *m* in equation (3).

Pointing loss
Pointing loss is due to pointing, acquisition and tracking (PAT) system errors and reflector random movements. The pointing loss L_{PNT} is[49],

$$L_{PNT} = exp(-8\theta_j^2/w_0^2) \tag{10}$$

where θ_j is the pointing jitter's divergence angle in rad[1].

Scintillation loss
Scintillation loss is caused by thermal variations in the atmosphere, which lead to refractive index changes. This loss is minimal but should be accounted for. Following the derivation in[50], the scintillation loss in *dB* can be expressed as

$$\begin{aligned} L_{\mathrm{SCI}} = 4.343 \times \Big[\mathrm{erf}^{-1}(2p_0 - 1) \cdot \Big[2\ln(\sigma_I^2 + 1)\Big]^{\frac{1}{2}} \\ - \frac{1}{2}\ln(\sigma_I^2 + 1)\Big] \end{aligned} \tag{11}$$

where p_o is a loss fraction region that occurs when the actual receiving power falls below a certain threshold of the mean power. No encoded quantum information can be decoded while the receiving power lies within this region, so the channel is modelled as either on or off. Channel coding and interleaving can recover the data lost in this region. We set $p_o = 0.01$ by following previous work[18,51]. Here σ_I^2 is the scintillation index for the receiving telescope given by,

$$\sigma_I^2 = A_{D_r} \times \sigma_{I,point}^2 \tag{12}$$

where A_{D_r} represents the aperture averaging factor and $\sigma_{I,point}^2$ is the scintillation index of a point receiver given by[52],

$$\sigma_{I,\mathrm{point}}^2 = \exp(A + B) - 1 \tag{13}$$

with,

$$A = \frac{0.49\sigma_R^2}{\left(1 + 1.11\sigma_R^{12/5}\right)^{7/6}}, \quad B = \frac{0.51\sigma_R^2}{\left(1 + 0.69\sigma_R^{12/5}\right)^{5/6}}$$

and,

$$A(D_r) = \left[1 + 1.062\left(\frac{D_r}{2\rho_I}\right)^2\right]^{-7/6} \tag{14}$$

Here ρ_I is the intensity structure parameter given by,

$$\rho_I = 1.5\sqrt{\frac{\lambda}{2\pi}H_d\left(\frac{\theta/90^\circ}{(\theta/90^\circ)^2 + (10/90^\circ)^2}\right)} \tag{15}$$

where θ is the elevation angle of the transmitter (in degrees) and H_d is the height of the troposphere, which will be set to 12,000 *m* according to[53]. The term σ_R^2 is the Rytov variance, which represents the fluctuations in propagating light caused by a turbulence medium in terms of phase and amplitude[54]; it is calculated as[52],

$$\sigma_R^2 = 2.25k^{\frac{7}{6}}\sec^{\frac{11}{6}}(\alpha)\int_{H_{GS}}^{H_{Turb}} C_n^2(h)(1 - H_{GS})^{\frac{5}{6}}dh \tag{16}$$

where α (Fig. 2) is the zenith angle, H_{GS} is the height of the ground station (GS) above sea level (in *m*). H_{Turb} denotes the altitude of the turbulence layer above the ground station (in *m*), and $C_n^2(h)$ is the refractive index structure parameter (using the modified Hufnagel-Valley Model) given by[55],

$$\begin{aligned} C_n^2(h) = A_0 \exp\Big(-\frac{H_{GS}}{700}\Big)\exp\Big(\frac{H_{GS} - h}{100}\Big) \\ + 5.94 \times 10^{-53} h^{10}\Big(\frac{U_{rms}}{27}\Big)^2 \exp\Big(-\frac{h}{1000}\Big) \\ + 2.7 \times 10^{-16}\exp\Big(-h/1500\Big). \end{aligned} \tag{17}$$

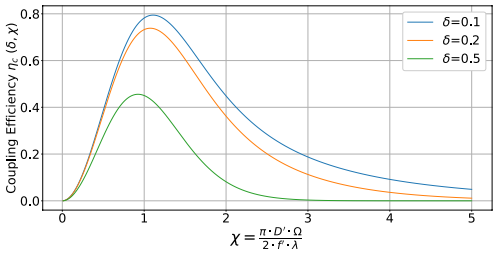

Fig. 9. The variation in the fibre coupling efficiency as a function of χ (equation (19)) for different pupil sizes to central obstruction sizes ratios δ.

Here A_0 is the refractive index structure parameter (RISP) at ground level (in $m^{-\frac{2}{3}}$), U_{rms} is the average wind speed along the slant path (in $m\ s^{-1}$). H_{Turb} is negligible above 20 *km*[51]; therefore, we do not consider the scintillation loss on the travel path *AB* when calculating the total loss.

Reflector losses

The parabolic reflector setup introduces fidelity-reducing factors in the quantum link due to various limitations, including construction imperfections such as surface aberrations, alignment issues, and non-ideal reflector shape. Additionally, hardware constraints, such as detector inefficiencies and fibre coupling losses, further degrade the fidelity, as described below. These factors are also considered in our design when calculating the channel loss, as applicable.

Fibre loss

For a Single Mode Fibre (SMF), the optical coupling efficiency (η_c) is given by[56],

$$\eta_c(\delta,\chi) = 2\left\{\frac{e^{-\chi^2}\left[1-e^{\chi^2(1-\delta^2)}\right]}{\chi\sqrt{1-\delta^2}}\right\}^2 \tag{18}$$

where

$$\chi = \frac{\pi \cdot D' \cdot \Omega}{2 \cdot f' \cdot \lambda}. \tag{19}$$

Here $D^{'}$ and $f^{'}$ are the lens diameter and focal length to the fibre, respectively, Ω is the beam radius at $1/e$ distance, and δ is the ratio between pupil size and central obstruction size (feed horn of the parabola in our case). For a $\delta = 0.1$, the coupling efficiency can be calculated as about 79% (Fig. 9), which gives L_{fibre} for the entire system (both transmitter and receiver) as,

$$L_{fibre} = -20 \cdot log_{10}(0.79) = 2.04\ dB \tag{20}$$

Figure 9, presents coupling efficiency, η_c, to the SMF as a function of χ for different δ values. It is evident that when $\delta = 0.1$, χ is approximately 1.108. Since ω_0 (in equation (4)) is a characteristic of the laser, for a chosen wavelength λ (1550 *nm* in our case), $D^{'}$ and $f^{'}$ must be selected to achieve the $\chi = 1.108$ for the maximum coupling efficiency of 79%. In addition, wavefront perturbations can also limit the coupling efficiency of the signal into an SMF[57]. However, it is not accounted for when modelling the reflector loss as the reflector is located in the stratosphere (at a 20 km altitude), which lies above the majority of atmospheric turbulence, where wavefront phase distortions are weaker and hence neglected.

Coating loss

This loss occurs as the coating material of the parabola (gold in our case) is not 100% reflective. Assuming the same hardware for both receiver and transmitter, we calculate the $L_{coating}$ for the entire system as[58],

$$\begin{aligned} L_{\text{coating}} &= -20 \cdot \log_{10}\left(\frac{I_{\text{reflected}}}{I_{\text{incident}}}\right) \\ &= -20 \cdot \log_{10}\left(\frac{\frac{1}{2}\epsilon\nu E_{\text{rf}}^2}{\frac{1}{2}\epsilon\nu E_{\text{i}}^2}\right) \\ &= -20 \cdot \log_{10}(r) \end{aligned} \tag{21}$$

where ϵ is the electric susceptibility, ν is the speed of light, and r is the reflectance of gold. E_{rf} and E_i represent the energies of the reflected and incident waves, respectively.

Lenses loss
Similarly, the loss due to imperfect transmittance through the onboard lens system L_{lenses} is given as

$$L_{lenses} = -20 \cdot log_{10}(t) \tag{22}$$

where t is the energy transmission efficiency of a single lens system (i.e., in the transmitter or receiver setup of the reflector).

Design loss
Assuming a more general value for the design efficiency of a parabola[35], we get the design loss (L_{desgin}) due to the imperfect construction of parabolas as,

$$L_{design} = -20 \cdot log_{10}(0.65) = 3.741\ dB \tag{23}$$

EGR, SKR, QBER, and Bell parameter calculation

The total path loss primarily affects the EGR, SKR, and QBER. These three parameters can be calculated using the transmission efficiency (η_{trans}) of the entire quantum link through the atmosphere, given by

$$\eta_{trans} = 10^{-T_{TOT}/10} \tag{24}$$

where T_{TOT} is the transmission loss (in dB) of the entire quantum channel with selected transmission method as calculated under case I (L_{ABC}), II (L_{AB}), or III (L_{AC}). The section below details SKR and QBER for the BB84 protocol, as well as Bell parameter and EDR calculations for the E91 protocol. Although we consider detector efficiencies in our calculations below, we do not consider fibre coupling efficiencies at the ground station assuming free-space coupling for detection, where the received beam from the telescope is directly focused onto the detector, for simplicity as well as to support our primary objective of studying the effect of the reflector.

BB84 protocol

In the BB84 protocol[29], where the satellite directly communicates with one ground station, the error in the transmitted key can be calculated using the QBER (Q_{BB84}), which is given by[59],

$$Q_{BB84} = q_i + 0.5\frac{P_{nc}n}{\eta_{trans}\eta_{det}q\mu} \tag{25}$$

where q_i is the intrinsic QBER defining the optical quality of the optical system being used, typically 0.001 for a commercial detector, P_{nc} is noise count probability, n is the number of detectors, q is the parameter used to correct non-interfering path combinations (this is either 1 or 0.5, and we set it to 0.5), μ is the mean photon number (1 for single photon source), and η_{det} is the efficiency of the detector[60]. Using the QBER (Q_{BB84}), the SKR for the BB84 (SKR_{BB84}) protocol can be calculated as,

$$\begin{aligned} SKR_{\mathrm{BB84}} = \frac{1}{2}\nu_s \cdot \eta_{\mathrm{trans}} \Big[& 1 + 2Q_{\mathrm{BB84}} \log_2(Q_{\mathrm{BB84}}) \\ & + 2(1 - Q_{\mathrm{BB84}}) \log_2(1 - Q_{\mathrm{BB84}}) \Big] \end{aligned} \tag{26}$$

where ν_s is the photon generation rate at the satellite, which is set to 5.9 *MHz* following real-world values from the Micius experiment[61].

E91 protocol
In the E91 protocol[30], we assume that the satellite generates two entangled photons sent through the atmosphere towards Alice and Bob, two separate ground stations, one of which is shown in Fig. 2. Between two distributed photons, the maximally entangled state is given by[60],

$$\psi\rangle = \frac{1}{\sqrt{2}}\left(|H\rangle_A|V\rangle_B + e^{i\varphi}|V\rangle_A|H\rangle_B\right)$$

where φ is the relative phase, H and V are the horizontal and vertical polarisations of the photon pair, respectively. The quality of entanglement between photon pairs in the E91 state is assessed using the degree of violation of a Bell inequality using the Clauser–Horne–Shimony–Holt (CHSH) inequality. For such a case, the Bell parameter S_{CHSH} is calculated as[30],

$$\begin{aligned} S_{\mathrm{CHSH}} = \Big| & E(\theta_A^i, \theta_B^i) + E(\theta_A^i, \theta_B^j) \\ & - E(\theta_A^j, \theta_B^i) + E(\theta_A^j, \theta_B^j) \Big| \end{aligned} \tag{27}$$

where $E(\theta_A^i, \theta_B^j)$ is the correlation coefficient representing two different random orientations, i and j ($i,\ j \in \mathbb{Z}^+$), of Alice's and Bob's analysers, given by[62],

$$E(\theta_A, \theta_B) = N\Big[-\cos(2\theta_A)\cos(2\theta_B) + \cos(\varphi)\sin(2\theta_A)\sin(2\theta_B)\Big] \tag{28}$$

With two random numbers for $i\ (=2)$ and $j\ (=4)$, it can be seen that at the relative phase angle $\varphi = \pi$ with orientation angles $(\theta_A^2, \theta_A^4, \theta_B^2, \theta_B^4) = (0, \frac{\pi}{4}, \frac{-\pi}{8}, \frac{\pi}{8})$, we obtain a maximum value[30] of $2\sqrt{2}$ for S_{CHSH}. We use these four orientation angles to study the impact of the noise parameter (N) on the Bell parameter, where

$$N = \frac{p_s \eta_t^2}{\kappa} \tag{29}$$

with

$$\kappa = p_s\left[\eta_t + 2P_{nc}(1-\eta_t)\right]^2 + 2p_1 P_{nc}\left[\eta_t + 2P_{nc}(1-\eta_t)\right] + 4p_0 P_{nc}^2$$

Let $\eta_{trans,A}$ and $\eta_{trans,B}$ be the transmission efficiencies for Alice and Bob respectively. We obtain $p_s = \eta_{trans,A} \cdot \eta_{trans,B}$, $p_1 = p_{HA} + p_{VA} + p_{HB} + p_{VB}$ with $p_{HA} = p_{VA} = 0.5 \cdot \eta_{trans,A} \cdot (1 - \eta_{trans,B}), p_{HB} = p_{VB} = 0.5 \cdot \eta_{trans,B} \cdot (1 - \eta_{trans,A})$ and $p_0 = (1 - \eta_{trans,A})(1 - \eta_{trans,B})$[62]. η_t is the total detection efficiency of the system, given by the product of detector efficiency (η) and photon collection efficiency (η_c) while P_{nc} is the probabilistic noise count[60]. For simplicity, we assume that $\eta_{trans,A} = \eta_{trans,B}$ in our case, where $\eta_{trans,A}$ was calculated according to the simulation parameters given in the Table. 1. However, even with $\eta_{trans,B} = 0.75 \cdot \eta_{trans,A}$, we noticed that there is only a small difference in minimum usable elevation angle for QKD with E91 protocol, while some noticeable difference between SKR values (refer to supplementary materials for more analytical results for $\eta_{trans,B} = c \cdot \eta_{trans,A}$ where $c \in \{0.75, 0.5, 0.25\}$). Using the derivation in[63], we calculate the QBER for the E91 protocol Q_{E91} as,

$$Q_{E91} = \frac{1}{2}\left(1 - \frac{S_{CHSH}}{2\sqrt{2}}\right) \tag{30}$$

and the SKR for the E91 (SKR_{E91}) protocol as,

$$SKR_{E91} = \frac{1}{3} v_s \cdot \eta_{\text{trans}}\left[1 - h(Q_{E91}) - h\left(f(s)\right)\right] \tag{31}$$

with

$$f(s) = \frac{1 + \sqrt{\frac{S_{CHSH}^2}{4} - 1}}{2}$$

where $h(x)$ is the Shannon entropy function[60] of x, given by,

$$h(x) = -x\log_2(x) - (1-x)\log_2(1-x); 0 \le x \le 1 \tag{32}$$

EDR calculation

We consider the same scenario for calculating EDR as we did when analysing the E91 protocol, with the satellite as an untrusted source. Considering channel transmittance for both ground stations, Alice and Bob, for a certain l_{path} into account (as explained in equation (24)), the average EDR to the ground stations without taking detector efficiencies into account (as we are interested in studying the effect of the reflector) is[64],,

$$EDR = v_s \cdot \eta_{trans} \tag{33}$$

Communication time window

Assuming a circular orbit, the communication time window for the secret key distribution for a certain sighting opportunity can be calculated up to the maximum elevation by dividing the angular displacement of the satellite by the satellite's angular velocity relative to the receiver (ground station or balloon). In general, the communication time window, T_{COMM} is,

$$T_{COMM} = \frac{\pi(90 - \theta_{min})}{180\omega} \tag{34}$$

where θ_{min} $(0 \leq \theta_{min} \leq 90^{\circ})$ is the elevation angle (in degrees) at the first instant that SKR becomes positive, and ω is the angular velocity of the satellite relative to the ground station or balloon in $rad\ s^{-1}$.

Data availability

The dataset analysed during the current study is available from the corresponding author upon reasonable request.

Code availability

The code that supports the findings of this study is available upon reasonable request.

Received: 11 March 2025; Accepted: 12 September 2025
Published online: 17 October 2025

References

1. Chu, Y., Donaldson, R., Kumar, R. & Grace, D. Feasibility of quantum key distribution from high altitude platforms. *Quantum Science and Technology* **6**, 035009. https://doi.org/10.1088/2058-9565/abf9ae (2021).
2. Sheng, Y.-B., Zhou, L. & Long, G.-L. One-step quantum secure direct communication. *Science Bulletin* **67**, 367–374 (2022). https://www.sciencedirect.com/science/article/pii/S2095927321006940.
3. Chen, Y.-A. et al. An integrated space-to-ground quantum communication network over 4,600 kilometres. *Nature* **589**, 214–219 (2021).
4. Martin, V. et al. Madqci: A heterogeneous and scalable sdn-qkd network deployed in production facilities (2024).
5. Gonzalez-Raya, T., Pirandola, S. & Sanz, M. Satellite-based entanglement distribution and quantum teleportation with continuous variables. *Communications Physics* **7**, 126 (2024).
6. Wengerowsky, S. et al. Entanglement distribution over a 96-km-long submarine optical fiber. *Proceedings of the National Academy of Sciences* **116**, 6684–6688 (2019). https://doi.org/10.1073/pnas.1818752116.
7. Zhao, P. et al. Quantum secure direct communication with hybrid entanglement. *Frontiers of Physics* **19**, 51201 (2024). https://journal.hep.com.cn/fop/EN/abstract/article_37779.shtml.
8. Pan, D. et al. The evolution of quantum secure direct communication: On the road to the qinternet. *IEEE Communications Surveys & Tutorials* **26**, 1898–1949 (2024).
9. Acosta, V. M. et al. Analysis of satellite-to-ground quantum key distribution with adaptive optics. *New Journal of Physics* **26**, 023039. https://doi.org/10.1088/1367-2630/ad231c (2024).
10. Yang, Y. et al. A 300-km fully-connected quantum secure direct communication network. *Science Bulletin* **70**, 1445–1451 (2025). https://www.sciencedirect.com/science/article/pii/S209592732500204X.
11. M. Lucamarini, J. F. D. . A. J. S., Z. L. Yuan. Overcoming the rate–distance limit of quantum key distribution without quantum repeaters. *Nature* **557**, 400–403 (2018).
12. Liu, Y. et al. Experimental twin-field quantum key distribution over 1000 km fiber distance. *Phys. Rev. Lett.* **130**, 210801 (2023). https://doi.org/10.1103/PhysRevLett.130.210801.
13. Sharma, V. & Banerjee, S. Analysis of atmospheric effects on satellite-based quantum communication: a comparative study. *Quantum Information Processing* **18**, 67. https://doi.org/10.1007/s11128-019-2182-0 (2019).
14. Liao, S.-K. et al. Satellite-to-ground quantum key distribution. *Nature* **549**, 43–47 (2017).
15. Yin, J. et al. Satellite-based entanglement distribution over 1200 kilometers. *Science* **356**, 1140–1144 (2017).
16. Ren, J.-G. et al. Ground-to-satellite quantum teleportation. *Nature* **549**, 70–73. https://doi.org/10.1038/nature23675 (2017).
17. Liao, S.-K. et al. Satellite-relayed intercontinental quantum network. *Phys. Rev. Lett.* **120**, 030501 (2018). https://doi.org/10.1103/PhysRevLett.120.030501.
18. Giggenbach, D. & Moll, F. Scintillation loss in optical low earth orbit data downlinks with avalanche photodiode receivers (2017).
19. Saathof, R. et al. Optical technologies for terabit/s-throughput feeder link (2017).
20. Avesani, M. et al. Full daylight quantum-key-distribution at 1550 nm enabled by integrated silicon photonics. *npj Quantum Information* **7**, 93 (2021). https://doi.org/10.1038/s41534-021-00421-2.
21. Sidhu, J. S. et al. Advances in space quantum communications. *PRX Quantum* **2**, 182–217. https://doi.org/10.1049/qtc2.12015 (2021).
22. Belenchia, A. et al. Quantum physics in space. *Physics Reports* **951**, 1–70 (2022). https://www.sciencedirect.com/science/article/pii/S0370157321004142. Quantum Physics in Space.
23. Islam, T. et al. Finite-resource performance of small-satellite-based quantum-key-distribution missions. *PRX Quantum* **5**, 030101 (2024). https://doi.org/10.1103/PRXQuantum.5.030101.
24. Vasylyev, D., Vogel, W. & Moll, F. Satellite-mediated quantum atmospheric links. *Phys. Rev. A* **99**, 053830 (2019).
25. Pirandola, S. Satellite quantum communications: fundamental bounds and practical security. *Phys. Rev. Res.* **3** (2021).
26. Sidhu, J. S., Brougham, T., McArthur, D., Pousa, R. G. & Oi, D. K. L. Finite key effects in satellite quantum key distribution. *npj Quantum Information* **8** (2022). https://doi.org/10.1038/s41534-022-00525-3.
27. Lanning, R. N., Harris, M. A., Oesch, D. W., Oliker, M. D. & Gruneisen, M. T. Quantum communication over atmospheric channels: A framework for optimizing wavelength and filtering. *Phys. Rev. Appl.* **16**, 044027 (2021). https://doi.org/10.1103/PhysRevApplied.16.044027.
28. Gruneisen, M. T. et al. Adaptive-optics-enabled quantum communication: A technique for daytime space-to-earth links. *Phys. Rev. Appl.* **16**, 014067 (2021). https://doi.org/10.1103/PhysRevApplied.16.014067.
29. Bennett, C. H. & Brassard, G. Quantum cryptography: Public key distribution and coin tossing. *Theoretical Computer Science* **560**, 7–11 (2014). https://www.sciencedirect.com/science/article/pii/S0304397514004241. Theoretical Aspects of Quantum Cryptography – celebrating 30 years of BB84.
30. Ekert, A. K. Quantum cryptography based on bell's theorem. *Phys. Rev. Lett.* **67**, 661–663 (1991). https://doi.org/10.1103/PhysRevLett.67.661.
31. Malinowski, A. & Zielinski, R. High altitude platform - future of infrastructure. *International Journal of Electronics and Telecommunications* **56** (2010).
32. Rahmat-Samii, Y. *Reflector Antennas* (Springer US, Boston, MA, 1988). https://doi.org/10.1007/978-1-4615-6459-1_15.
33. Balanis, C. A. *Antenna theory: Analysis and design* 3rd edn (John Wiley, 2005).
34. Zaïm, A. Understanding the physics and functioning of parabolic antennas: A concise overview (2023).
35. Nikolova, N. K. Lecture 19: Reflector antennas (2016). https://www.ece.mcmaster.ca/faculty/nikolova/antenna_dload/current_lectures/L19_Reflector.pdf. Accessed: 2024-06-27.
36. Şerbescu, H., Sandu, C., Vintila, S., Radu, A. & Niculescu, F. Development of a parabolic mirror using advanced materials used for an environment friendly propulsion system. *AIP Conference Proceedings* **2022**, 020005. https://doi.org/10.1063/1.5060685 (2018).

37. Morozov, S., Gaio, M., Maier, S. A. & Sapienza, R. Metal–dielectric parabolic antenna for directing single photons. *Nano Letters* **18**, 3060–3065. https://doi.org/10.1021/acs.nanolett.8b00557 (2018) (**PMID: 29595270**).
38. Raney, K. *Radar, Altimeters* (Springer New York, New York, NY, 2014). https://doi.org/10.1007/978-0-387-36699-9_134.
39. Georgiev, K. *et al.* Metasurface dichroic mirrors: Application to low quantum defect lasers (2021). https://www.scopus.com/pages/publications/85117587678?inward=. Cited by: 0.
40. Arnold, N. T., Lualdi, C. P., Goggin, M. E. & Kwiat, P. G. All-optical quantum memory (2024).
41. Loebich, O. The optical properties of gold. *Gold Bulletin* **5**, 2–10. https://doi.org/10.1007/BF03215148 (1972).
42. Yin, J. et al. Satellite-based entanglement distribution over 1200 kilometers. *Science* **356**, 1140–1144 (2017). https://doi.org/10.1126/science.aan3211.
43. Rabah, K. Implementation of one-time pad cryptography. *Information Technology Journal* **4**, 87–95 (2005).
44. Shu, H. Asymptotically optimal prepare-measure quantum key distribution protocol. *International Journal of Theoretical Physics* **62** (2023).
45. Lu, C.-Y., Cao, Y., Peng, C.-Z. & Pan, J.-W. Micius quantum experiments in space (2022).
46. Behl, A., Bhatia, A. & Puri, A. Parabolic antennas and its applications. *International Journal of Innovative Research in Technology* **1**, 2117–2121 (2014). https://ijirt.org/publishedpaper/IJIRT101028_PAPER.pdf. Accessed: 2025-07-19.
47. Moision, B. et al. Demonstration of free-space optical communication for long-range data links between balloons on project loon (2017).
48. Long, R. Atmospheric attenuation of ruby lasers. *Proceedings of the IEEE* **51**, 859–860 (1963).
49. Kaushal, H., Jain, V. K. & Kar, S. *Free Space Optical Communication* Optical Networks (Springer, Singapore, 2017). https://doi.org/10.1007/978-81-322-3691-7.
50. Giggenbach, D. & Henniger, H. Fading-loss assessment in atmospheric free-space optical communication links with on-off keying. *Optical Engineering* **47**, 046001–1 (2008).
51. Ntanos, A. et al. Leo satellites constellation-to-ground qkd links: Greek quantum communication infrastructure paradigm. *Photonics* **8** (2021). https://www.mdpi.com/2304-6732/8/12/544.
52. Andrews, L. & Phillips, R. *Laser Beam Propagation through Random Media* (SPIE Optical Engineering Press, 1998).
53. Andrews, L. C., Phillips, R. L. & Young, C. Y. Scintillation model for a satellite communication link at large zenith angles. *Optical Engineering* **39** (2000).
54. Andrews, L. C., Phillips, R. L. & Hopen, C. Y. *Laser beam scintillation with applications* Vol. 99 (SPIE press, 2001).
55. Kapsis, T. T., Lyras, N. K., Kourogiorgas, C. I. & Panagopoulos, A. D. Time series irradiance synthesizer for optical geo satellite downlinks in 5g networks. *Future Internet* **11** (2019). https://www.mdpi.com/1999-5903/11/6/131.
56. Gruneisen, M. T., Flanagan, M. B. & Sickmiller, B. A. Modeling satellite-Earth quantum channel downlinks with adaptive-optics coupling to single-mode fibers. *Optical Engineering* **56**, 126111. https://doi.org/10.1117/1.OE.56.12.126111 (2017).
57. Scriminich, A. et al. Optimal design and performance evaluation of free-space quantum key distribution systems. *Quantum Science and Technology* **7**, 045029. https://doi.org/10.1088/2058-9565/ac8760 (2022).
58. Serrede, P. Lecture notes 6: Electromagnetic waves in matter (2005). https://hep.physics.illinois.edu/home/serrede/P436/Lecture_Notes/P436_Lect_06.pdf. Accessed: 2024-07-09.
59. Gisin, N., Ribordy, G., Tittel, W. & Zbinden, H. Quantum cryptography. *Rev. Mod. Phys.* **74**, 145–195 (2002). https://doi.org/10.1103/RevModPhys.74.145.
60. Sisodia, M., Omshankar, Venkataraman, V. & Ghosh, J. Fso-qkd protocols under free-space losses and device imperfections: a comparative study. *Quantum Information Processing* **23**, 185 (2024). https://doi.org/10.1007/s11128-024-04382-1.
61. Yin, J. et al. Entanglement-based secure quantum cryptography over 1,120 kilometres. *Nature* **582**, 501–505 (2020).
62. Semenov, A. A. & Vogel, W. Entanglement transfer through the turbulent atmosphere. *Physical Review A* **81** (2010). https://doi.org/10.1103/PhysRevA.81.023835.
63. Acín, A. et al. Device-independent security of quantum cryptography against collective attacks. *Phys. Rev. Lett.* **98**, 230501 (2007). https://doi.org/10.1103/PhysRevLett.98.230501.
64. Khatri, S., Brady, A. J., Desporte, R. A., Bart, M. P. & Dowling, J. P. Spooky action at a global distance: analysis of space-based entanglement distribution for the quantum internet. *npj Quantum Information* **7**, 4 (2021).

Acknowledgements

This publication has emanated from research conducted with the financial support of Taighde Éireann – Research Ireland under Grant number 13/RC/2077_P2 at CONNECT: the Research Ireland Centre for Future Networks and under Grant number 21/US-C2C/and from the US National Science Foundation under Grants CNS-2402861 and EEC-1941583.

Author contributions

K.S., D.T., and D.K. wrote the main manuscript, and K.S. generated the figures. N.K. contributed by providing theoretical points of view about atmospheric transmission losses. A.W. contributed by providing concepts for hybrid communication/post-quantum cryptography methods. All authors reviewed the manuscript.

Declarations

Competing interests

The authors declare no competing interests.

Additional information

Supplementary Information The online version contains supplementary material available at https://doi.org/10.1038/s41598-025-20273-6.

Correspondence and requests for materials should be addressed to K.S.